MGPB

Geophysical investigations of a potential landslide area in Mayoon, Hunza District, Gilgit-Baltistan, Pakistan

Rudarsko-geološko-naftni zbornik
(The Mining-Geology-Petroleum Engineering Bulletin)
UDC: 550.3
DOI: 10.17794/rgn.2021.3.9

Original scientific paper

Qasim ur Rehman[1,2], Waqas Ahmed[1], Muhammad Waseem[3], Sarfraz Khan[1], Asam Farid[4], Syed Husnain Ali Shah[5]

[1] *National Centre of Excellence in Geology, University of Peshawar, Pakistan.*
[2] *Department of Earth Sciences, University of Haripur, Pakistan.*
[3] *Department of Civil Engineering Peshawar Campus, University of Engineering and Technology Peshawar, Pakistan.*
[4] *Geophysical Technical Unit Arab Com Engineering & Soil, Al Khobar Saudi Arabia.*
[5] *Department of Earth and Environmental Sciences, Hazara University Mansehra, Pakistan.*

Abstract

The Mayoon landslide in the Hunza District is a slowly developed, non-catastrophic landslide that has gained its importance in the last few years after its rapid activation and fast slip rate. The area is characterized by high earthquake hazards (zone 3 with a peak ground acceleration value of 2.4–3.2 m/s^2) by the Building Code of Pakistan due to frequent earthquakes. The past high earthquake activity in the area has displaced the foliated rocks towards the south and is responsible for opening the bedrock joints. The head and body of the landslide are covered by unconsolidated material and have fractures of varying lengths and widths. The non-invasive geophysical techniques, including Ground Penetrating Radar (GPR) and Electrical Resistivity Soundings (ERS), are deployed to evaluate the Mayoon landslide subsurface. The subsurface is interpreted into a two-layer model. Bright reflectors and highly variable resistivity characterize the top layer (Layer-1). This layer is associated with a loose, highly heterogeneous, fragmented material deposited under glacial settings over the existing bedrock. Hyperbolic reflections and intermediate resistivity characterize the bottom layer (Layer-2). This layer is associated with foliated metamorphic bedrock. The hyperbolic reflections show faults/fractures within the bedrock. The extension of these fractures/faults with depth is uncertain due to decay in the GPR signal with depth. The intermediate resistivity shows the bedrock is weathered and foliated. Reflections within Layer-1 have disrupted directly above the fractures/faults suggesting a possible movement. A bright reflection between the two layers highlights the presence of the debonded surface. Loose material within Layer-1 coupled with debonding possesses a significant hazard to generate a landslide under unfavourable conditions, such as an intense rainstorm or earthquake activity.

Keywords:
GPR and ERS, Mayoon, hyperbolic reflections, debonded surface, foliated bedrock

1. Introduction

North Pakistan territory gains its uniqueness in hosting younger mountain belts, glaciated peaks, rugged topography, deeply incised valleys, and multiple mountain hazards. Hunza-Nagar Valley in North Pakistan is located in the Karakoram Mountain range and is strongly affected by devastating landslides (**Bacha et al., 2018**). The National Disaster Management Authority (NDMA) of Pakistan has marked the area as highly vulnerable to flash floods, avalanches, and landslides. Landslides are a frequent mountain hazard that pose a great threat to the community and infrastructure. The understanding of the deformation mechanism of a landslide improves our knowledge of its episodic evolution. This evolution depends on various factors, such as hydrology, tectonics, seismic activity, structure, climate (rainfall), rugged topography, and anthropogenic interference (**Regmi et al., 2017; Xie et al., 2020**). In the last decade, many studies have discussed the evolution and development of large landslides (**e.g. Dortch et al., 2009; Gallo and Lavé, 2014; Hewitt, 1998; Shang et al., 2003; Xie et al., 2020**). These studies focused on the recent and historic, catastrophic failures with massive transported deposits. Alternatively, slowly developing (30–50 years) non-catastrophic failures of high magnitude and low frequency can also be a severe threat to life and property (**Jones, 1992**). Such failures are mainly observed in highly sheared and foliated metamorphic rocks at higher altitudes (**Agliardi et al., 2013**). The behaviour of the landslide is affected by the material characterization and movement mechanism. The mass movement in the presence of a distinct weak zone separating the slide material from underlying stable material can be categorized as a translational or rotational landslide (**Hungr et al., 2014**).

Corresponding author: Qasim ur Rehman
qrehman@uoh.edu.pk

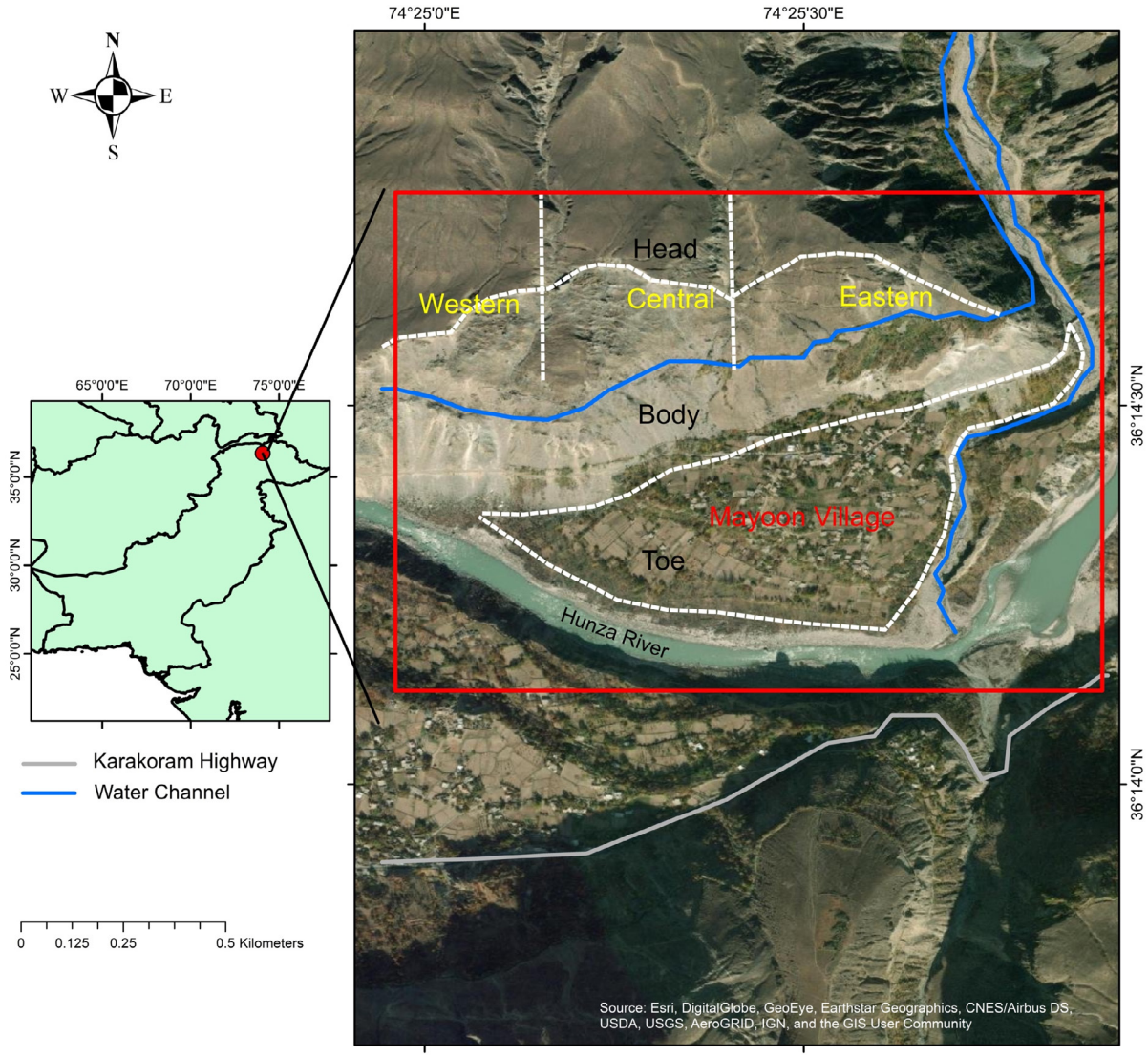

Figure 1: Location map of Mayoon Village, Hunza (Gilgit-Baltistan), Pakistan

The Mayoon Landslide is a non-catastrophic landslide located adjacent to Karakoram Highway and Mayoon Village, Hunza District, Gilgit Baltistan (see **Figure 1**). It covers a total area of 1500 m^2 that is continuously increasing since its first activation in 1976 (**Khan et al., 2019**). According to the residents, initially, it only damaged a few acres of land. After a long-dormant period, recent triggering episodes were recorded in 2010, 2011, and 2012, associated with heavy rainfall, seismic activity, and steep angles, instigating the evacuation of 20 families. In August and September 2020, the landslide's eastern side triggered twice and damaged farmland, two houses, and the local playground. The community residing at the toe of the landslide, i.e. 120 families, almost 1000 people, a secondary school, and a few shops, are all at risk of the landslide hazard (**Rehman et al., 2020**). A man-made water channel runs through the middle of the mountain and is used to supply water for the community residing in the next village. This landslide can also potentially destroy the existing China Pakistan Economic Corridor (CPEC) route, i.e. Karakoram Highway, and create a dam similar to Attabad Lake.

Recently, field investigations and remote sensing techniques are utilized in the study area to determine the risk and slip rate associated with the site (**Khan et al., 2019; Rehman et al., 2020**). Based on the InSAR data of over two years, (**Rehman et al., 2020**) found the maximum deformation rate as 20 mm/yr. and marked the Mayoon landslide as the second most active potential hazard site after the Gulmet landslide in Hunza Valley. However, no studies were performed regarding the evaluation of the internal structure of the Mayoon landslide. The geophysical tools and techniques provide an effective framework to investigate the internal structure, water content, and bedrock delineation of the landslide (**Ahmed et al., 2020; Ling et al., 2016; Meric et al., 2005; Mondal et al., 2008**). The Ground Penetrating Radar (GPR), a non-invasive geophysical technique, has been successfully deployed for potential hazard site characterization (**Borecka et al., 2015; Kannaujiya et**

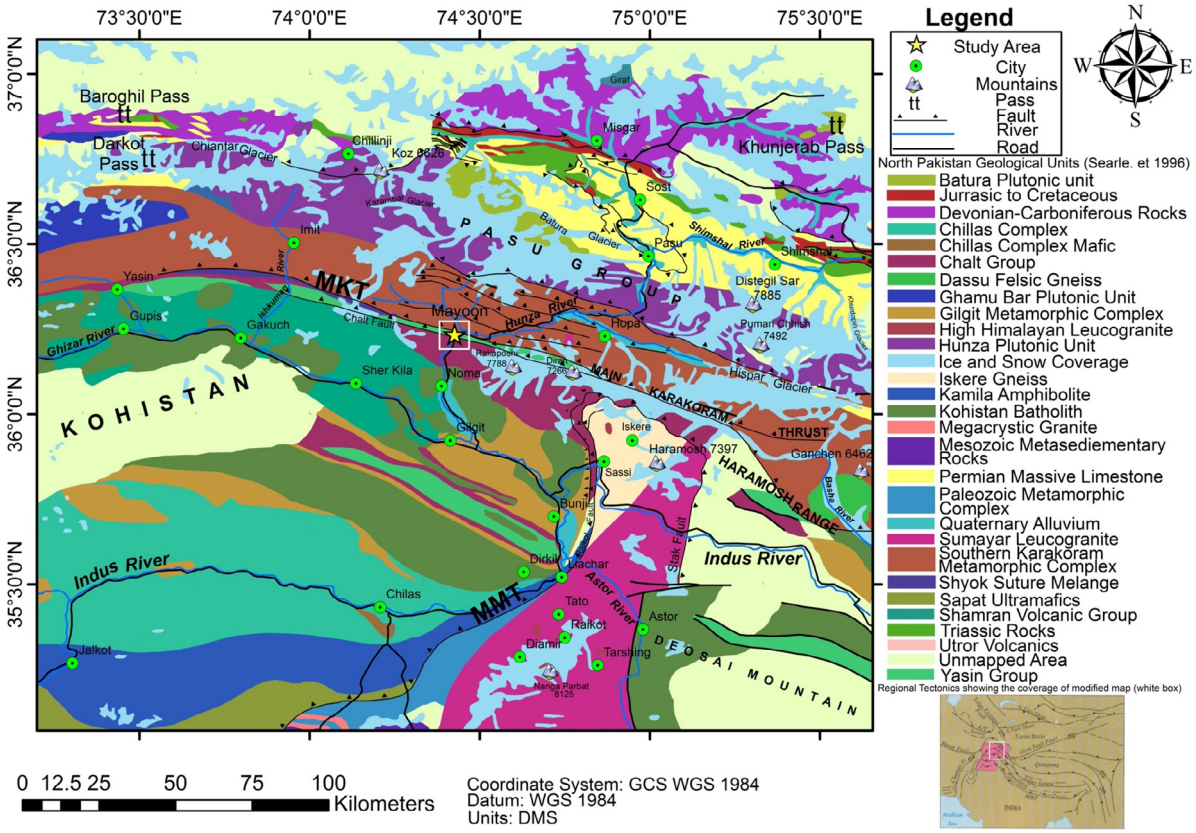

Figure 2: Geological map of North Pakistan (modified after **M.P, Searle and M.A, Khan 1996**)

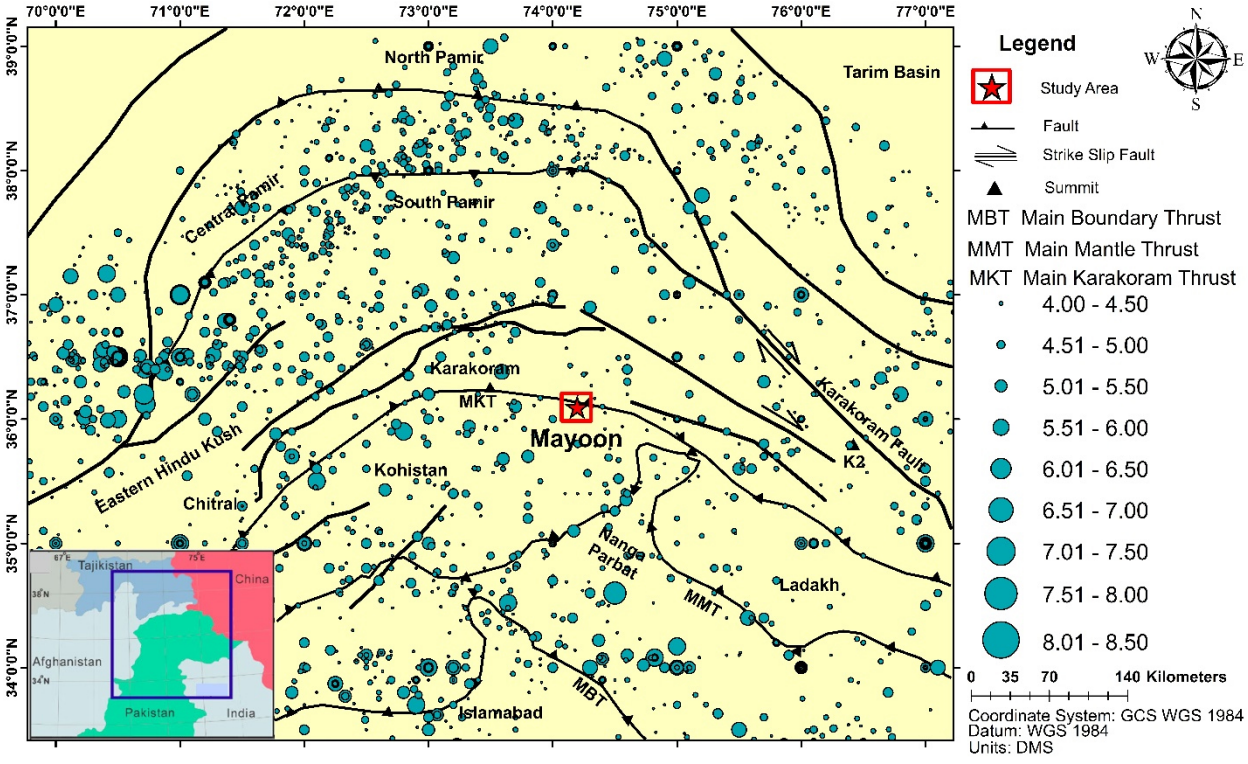

Figure 3: Regional tectonic map of North Pakistan showing active faults and major earthquake events in the region (**ISC Earthquake Catalogue, 2020**)

al., 2019; Lissak et al., 2015). The subsurface fractures, faults, and cavities are the target GPR monitors. The GPR has setback recognition to evaluate landslides due to; 1) high resolution; 2) high depth of penetration in resistive materials; and 3) sensitivity to magnetic, electric, and dielectric contrast (**Jongmans and Garambois, 2007**). Similarly, the non-invasive electrical resistivity technique can be used to characterize potential landslides (**Cardarelli and De Donno, 2017; Perrone et al., 2014; Yalcinkaya et al., 2016**). The Electrical Resistivity Surveying (ERS) method is based on measuring potential differences encountered at one pair of electrodes. At the same time, the current is injected into the subsurface with another pair of electrodes. The Vertical Electrical Sounding (VES) technique can be used to obtain vertical variation in resistivity. At the same time, the electrode array can be extended laterally to achieve larger depths. (**Telford et al., 1990**).

This study provides near-surface characterization of the Mayoon landslide by incorporating the GPR and ERS geophysical techniques to address the site's hazards. This study evaluates the internal structure of the landslide in terms of bedrock depth, faults and fractures density in the subsurface, and associated debonded surface with the overlying loose, fragmented material.

2. Geological and geographical setting

The study area has strategic importance in the Hunza District, Gilgit Baltistan. The Karakoram Highway (KKH) is a few hundred meters away from Mayoon Village. This is the only road connecting China and Pakistan. The China Pakistan Economic Corridor (CPEC) project, worth US $46 billion (**Hussain and Hussain, 2017; Irshad, 2015**) has also utilized the existing old Silk Road (KKH) for trade and tourism between China, Pakistan, and beyond (**Makhdoom et al., 2018**). The route is highly vulnerable to hazards and risks caused by landslides (**Ali et al., 2019**). The Mayoon landslide is a potential threat to KKH.

The region is characterized by active tectonics caused by the collision between the Indian and Eurasian plates (**Dewey et al., 1989; Searle et al., 1987**). Tectonically, the study area lies at the northern margin of the Kohistan Island Arc (KIA), bounded between the Main Karakoram Thrust, MKT (the mélange zone), and the Chalt Fault (see **Figure 2**). The KIA is formed due to intra-oceanic subduction within the Tethys Ocean before the collision of the Indian and Eurasian plates (**Jagoutz and Schmidt, 2012**). The KIA is welded to the Indian plate, marked by the Indus suture zone (Main Mantle Thrust, MMT) to the south and Eurasian plate by MKT to the north (**Bignold and Treloar, 2003**). The Karakoram-Himalayan thrust zone is categorized into four tectono-stratigraphic units from south to north, i.e. (1) Himalayan Crystalline zone; (2) Nangaparbat-Haramosh Massif; (3) Kohistan Magmatic belt; and (4) Karakoram Fold belt (**Searle et al., 1999**). The region is bound by major faults such as the Main Frontal Thrust (MFT), Main Boundary Thrust (MBT), Main Central thrust (MCT), Main Karakoram Thrust (MKT), South Tibetan detachment system (STD), and the dextral Karakoram fault system (**DiPietro and Pogue, 2004; Zanchi and Gaetani, 2011**).

The study area is composed of metamorphic rocks such as slates, phyllites, and schists of the Yasin metasedimentary group (Cretaceous-Paleocene). The basaltic rocks of the Chalt group and Quaternary deposits, including glacial moraines, glacial tills, glacial scree, and flood plain deposits are present (**Petterson, 2010; Zanchi and Gaetani, 2011**). Sediments of various origins such as lacustrine, colluvium, alluvium, and aeolian are unevenly distributed across Hunza Valley. These unconsolidated deposits have varying thicknesses ranging from a few meters to tens of meters and unconformably lie above the deformed bedrock across the area. Rugged topography with steep slopes, lack of vegetation, enormous unconsolidated scree encompassed by deep river valleys depict the geomorphology of the area and define the potential of large-scale landslides (**Rehman et al., 2020**). **Figure 3** shows the region's strong motion data from the year 25 AD-2020, with homogenized moment magnitude values ranging from Mw 4.0-8.5. The foliated rocks of the region placed at steep slopes were shaken several times during the past seismic activity and displaced the rocks towards the south of MKT. The active tectonics of the region are also responsible for the opening of cracks/fractures within the rocks exposed on the surface and the subsurface. The induced seismicity in the region with such geomorphology has amplified the landslide activity.

3. Methodology

The geophysical survey was planned after a reconnaissance of the site. The potential hazard sites were identified and marked before carrying out ERS and GPR survey. The signal-to-noise ratio of the acquired data was enhanced by using the latest industry software.

3.1 Field Observations

The field observations confirm the presence of several lineaments on the surface with considerable offset, highly sheared rocks placed at the slope, and the presence of a water channel running through the centre of the mountain (see **Figure 4**). The geophysical techniques, i.e. ERS and GPR were chosen to evaluate the subsurface of the Mayoon landslide. The landslide head is comprised of east-west oriented multiple cracks with a substantial opening, ranging from 0.5m to 5m (see **Figure 4a**). The surface layers mainly exposed along the landslide's body are comprised of silty, clayey soil with chunks of transported coarse rock fragments. The silty or clayey soil usually has very low ultimate strength (**Shah et al,**

Figure 4: Field photographs of the Mayoon landslide, (a) surface cracks on the top eastern part of the landslide, (b) glacial scree deposits on the top eastern part of the landslide, (c) highly sheared deformed bedrock exposed along the buried water pipeline track, (d) fractures within the deformed bedrock exposed at the surface (e) extensometer showing the movement in the central part of the landslide, (f) open water channel along the eastern part of the landslide

2019; Shah et al, 2020a; Shah et al, 2020b). The top loose glacial scree is positioned at almost 90° and is a potential threat in case of any severe tectonic activity (see **Figure 4b**). The rocks exposed along the central part of the landslide are highly sheared and weak due to shaking caused by the region's frequent earthquakes. A water channel runs through the middle of the landslide that is used to supply water to the next village. This channel is open at the landslide's eastern and western sides, whereas the landslide's central part has a buried water pipeline (see **Figure 4c**). The highly sheared and fractured rocks have multiple crack openings exposed at the surface along the pipeline track (see **Figure 4d**). The landslide's active movement is made obvious by an installed extensometer at the top of the landslide's central-eastern part (see **Figure 4e**). The landslide's eastern side has an open water channel with continuous seepage into the clayey, silty topsoil, and foliated rocks (see **Figure 4f**). The settlement including, houses, fields, orchards, and forest, is mainly present at the toe of the landslide adjacent to the Hunza River. The western part of the landslide has boulders of various rock types at the base, transported from above.

3.2 Geophysical investigations

The two geophysical techniques, namely Ground Penetrating Radar (GPR) and Electrical Resistivity Sounding (ERS) were executed in the landslide area to characterize the potential hazard associated with it. The locations of GPR and ERS profiles are shown on the base map (see **Figure 5**). For the GPR survey, MALA GPR with a low frequency (50 MHz) unshielded antenna was deployed due to the irregular terrain. The existing walking tracks were used to acquire data using the 'hip chain' procedure, whereas the navigation of the profiles was acquired using a handheld Global Positioning System (GPS). Six GPR data profiles were acquired using a sampling interval of 512 nanoseconds [ns] and a window length of 1000 nanoseconds [ns]. The handheld GPS was used for navigating GPR lines. The equipment was taken to the start of the profile lines, using the described parameters, and the acquisition was started. The data was acquired in fixed intervals for each profile to get full coverage, which then joined to make one complete profile. The GPR survey was conducted on the landslide's body to verify the fracture density in the subsurface.

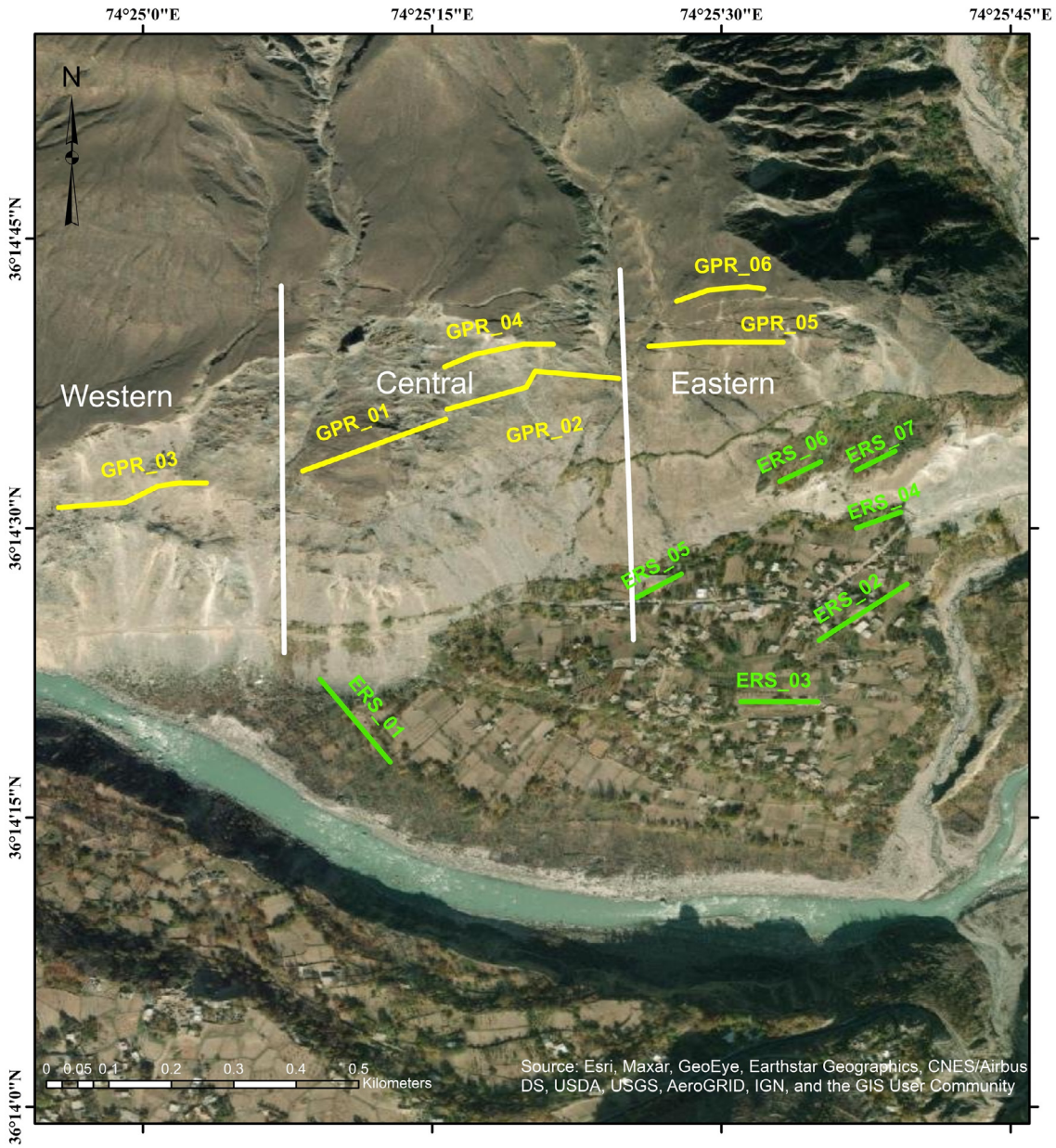

Figure 5: Base map with GPR and ERS locations presented on satellite imagery

The ERS was performed using the Terrameter SAS 4000 LUND Imaging System. The resistivity variation of the subsurface was obtained by using the Schlumberger configuration for current and potential electrodes. A total of seven ERS data profiles were acquired. The data was acquired in the available spaces, where electrode spread expansion was possible, such as along the walking tracks, farming field, and fruit yard terraces. The surface layer has a loose topsoil, intermixed with chunks of transported boulders having low-medium moisture contents. The current and potential electrode penetration was not good at the body and head of the landslide. Therefore, the ERS was opted at the toe of the landslide due to the gentle topography and moisturized topsoil cover.

3.3 Data Processing

The GPR data was processed with ReflexW software and then developed into GPR sections (**Alsharahi et al., 2016**). The processing procedure involved data loading and time adjustment to zero. The surface reflection interface was set to zero depth, and the global background was removed to enhance the coherent signal that reduces randomly varying signals. To convert the axis from two-way travel time into depth, 1D time to depth conversion was performed using the average velocity of 0.08 m/ns (according to the velocity analysis carried on the data). The colour palette was adjusted to signal amplitudes to improve the contrast of phase changes and signal variation.

The ERS data was processed using the standard routine procedures (assigning layers, resistivity, and inver-

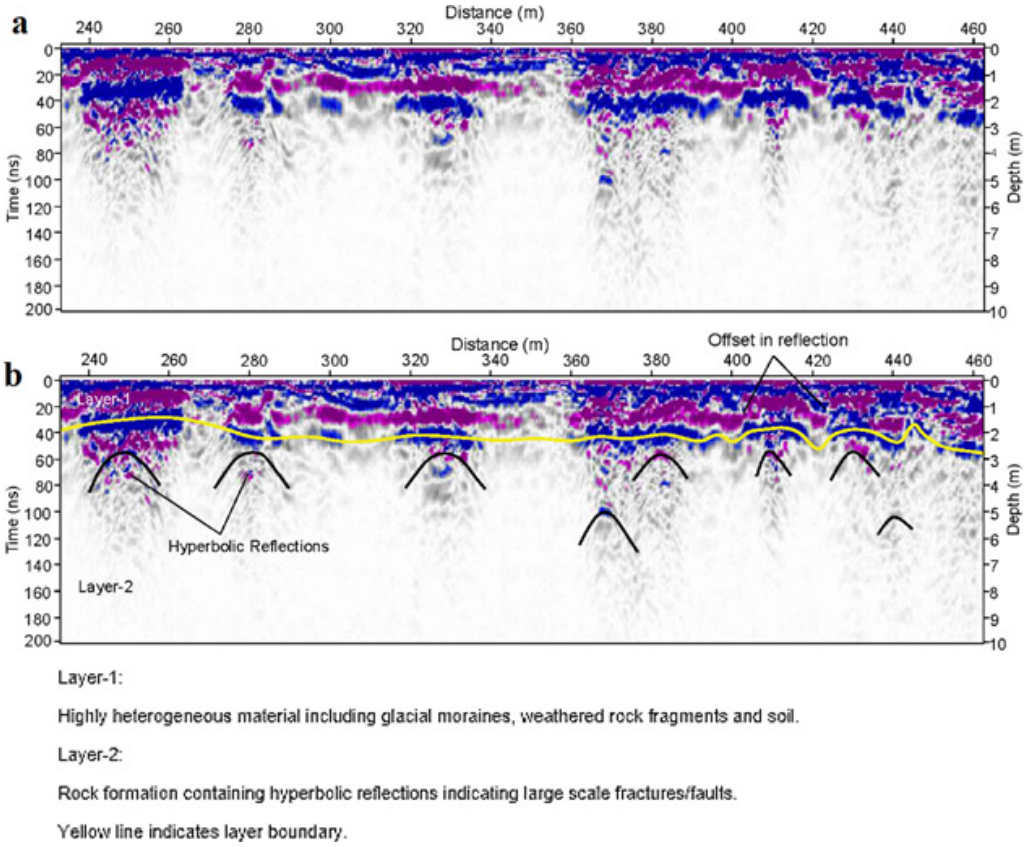

Figure 6: (a) Raw and (b) interpreted Ground Penetration Radar section for GPR_01

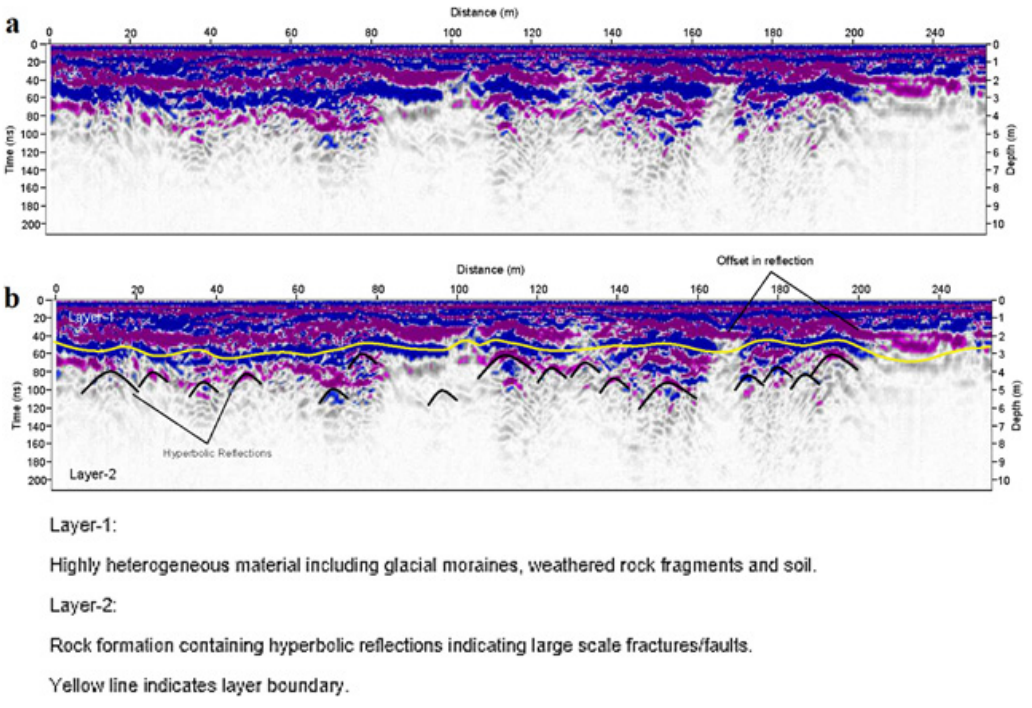

Figure 7: (a) Raw and (b) interpreted Ground Penetration Radar section for line GPR_02

sion for layered model) and developed into 1D subsurface profiles (**Brezhnev et al., 2020**). The initial ERS data processing involved the removal of spiky data and basic layer interpretation. Later on, this data (electrode spacing and corresponding resistivity values) was entered into the IPI2Win modelling software. Basic layers

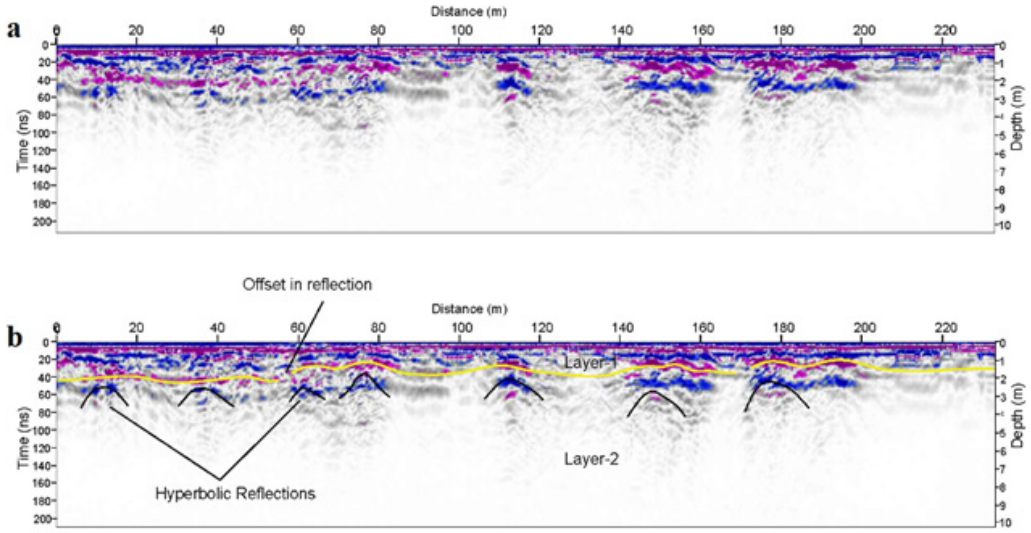

Layer-1:

Highly heterogeneous material including glacial moraines, weathered rock fragments and soil.

Layer-2:

Rock formation containing hyperbolic reflections indicating large scale fractures/faults.

Yellow line indicates layer boundary.

Figure 8: (a) Raw and (b) interpreted Ground Penetration Radar section for line GPR_03

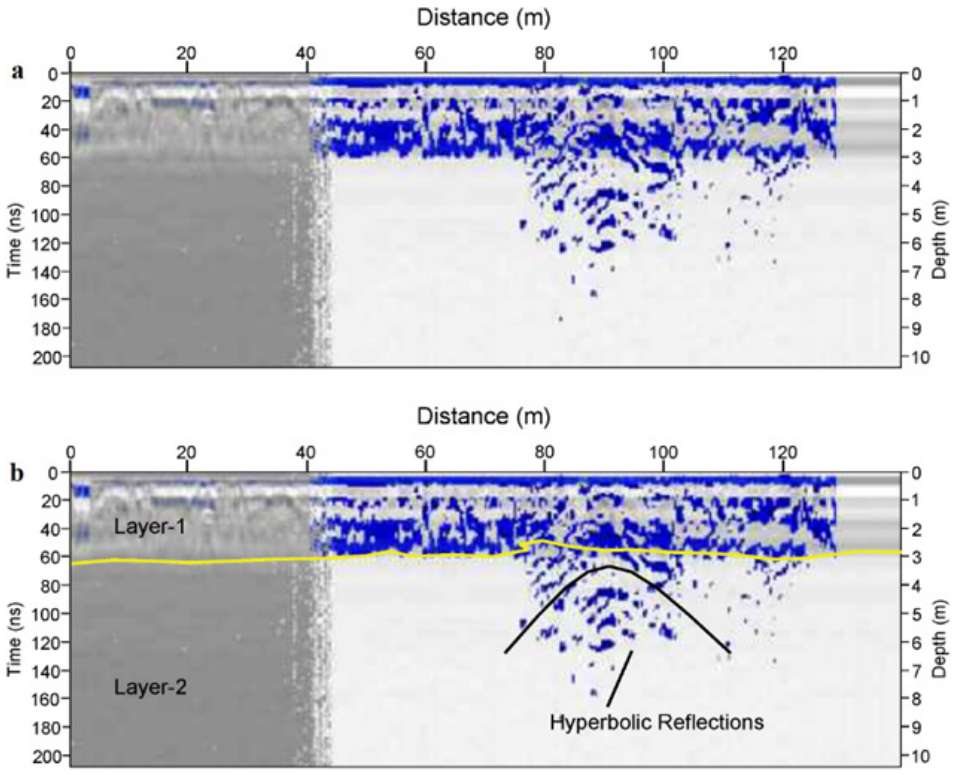

Layer-1:

Highly heterogeneous material including glacial moraines, weathered rock fragments and soil.

Layer-2:

Rock formation containing hyperbolic reflections indicating large scale fractures/faults.

Yellow line indicates layer boundary.

Figure 9: (a) Raw and (b) interpreted Ground Penetration Radar section for line GPR_04

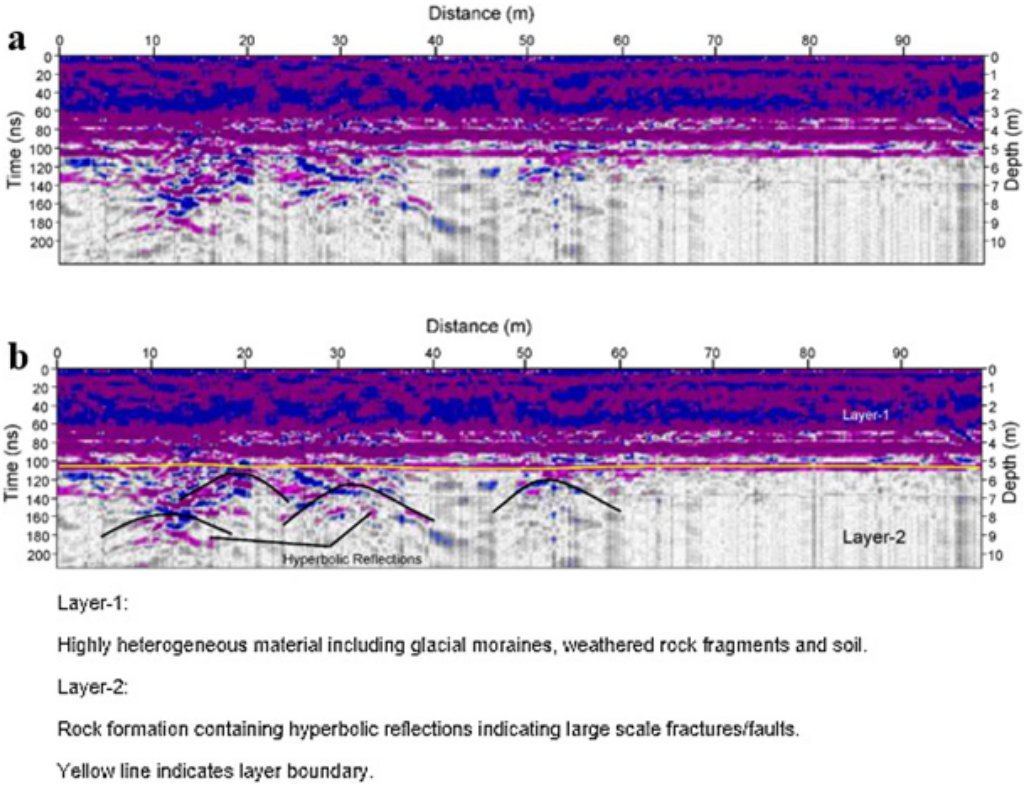

Figure 10: (a) Raw and (b) interpreted Ground Penetration Radar section for line GPR_05

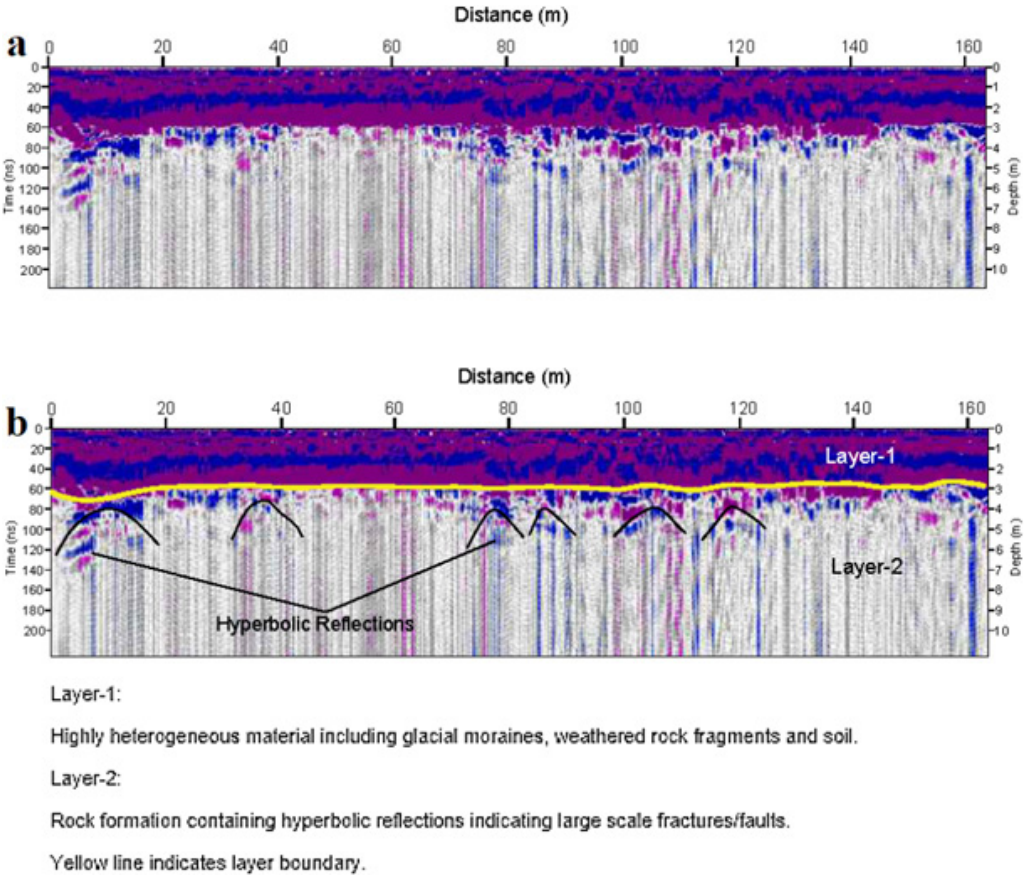

Figure 11: (a) Raw and (b) interpreted Ground Penetration Radar section for line GPR_06

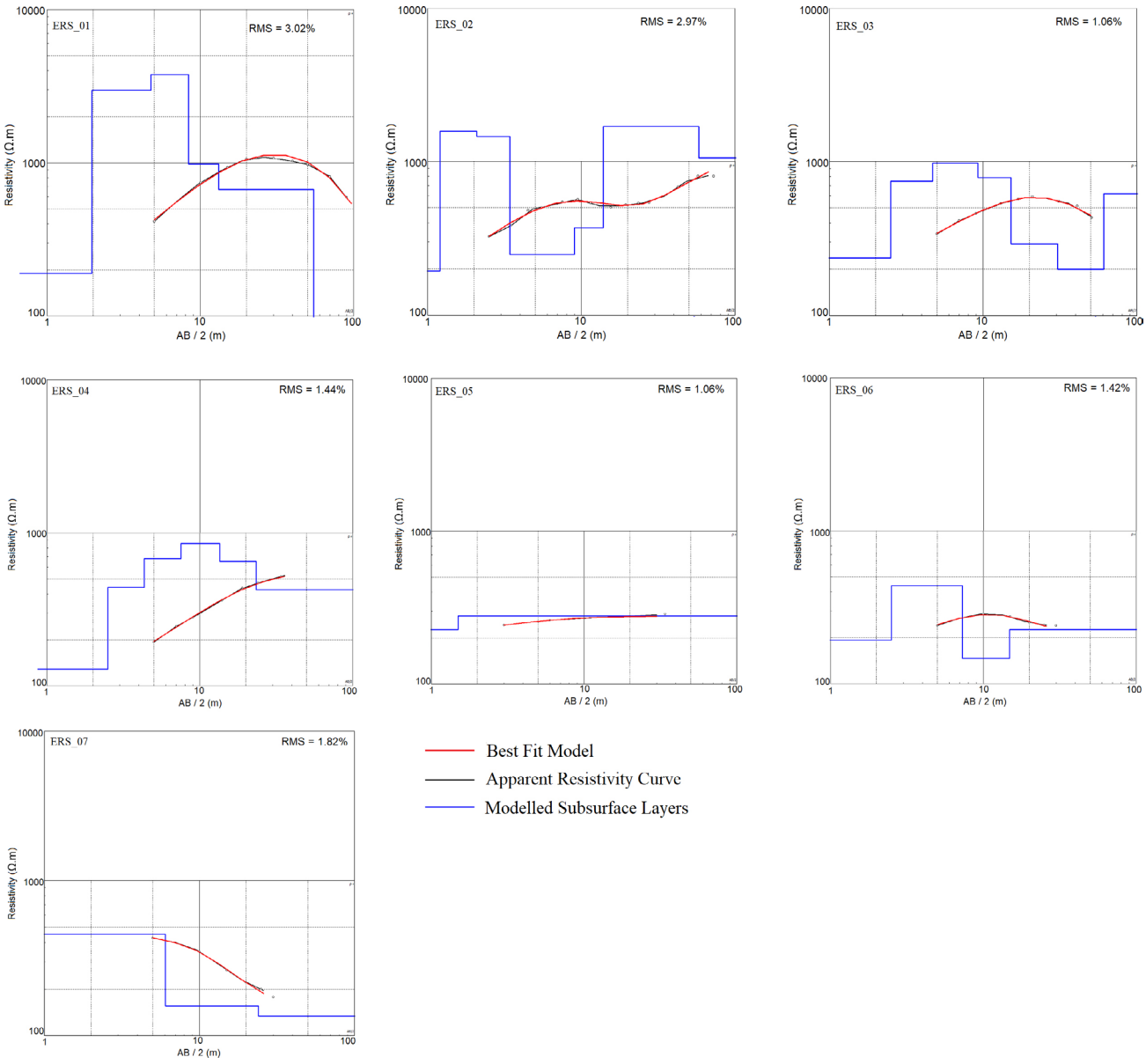

Figure 12: Field raw and processed ERS data (ERS_01 to ERS-07 profiles)

were defined before running the inversion program. Inversion was applied to a layered 1D model of the subsurface where minimum RMS error was reached.

4. Results

4.1 Ground Penetrating Radar (GPR)

The GPR_01 up to GPR_06 sections, represented by **Figures 6-11**, present the processed and interpreted GPR sections. The processed GPR sections were interpreted to show a two-layered subsurface model, i.e. top layer (Layer-1) and bottom layer (Layer-2). The boundary between Layer-1 and Layer-2 is highlighted by a yellow line in the interpreted GPR sections in **Figures 6-11**.

The GPR_01 section is shown in **Figure 6**. The section is interpreted as a two-layer case. The top layer is characterized by multiple reflections with high amplitudes representing different types of material i.e. silty-clayey soil, sand, and boulder size rock fragments with variable thickness. This material is the weathered product of the surrounding rocks which was deposited in situ and classified as soil horizons. Due to the variable thickness of different materials, GPR resulted in multiple reflections within the layer. Offsets in reflections are observed in Layer-1, which are indicative of below-lying fractures or lineaments. Layer-2 is interpreted to be associated with bedrock. It is characterized by relatively weak amplitudes and by many hyperbolic reflections primarily seen between horizontal distances 240-260 m, 275-285 m, 320-340 m, 365-385 m, 408-415 m, and 3-6m below ground level (BGL) (see **Figure 6**). The GPR signal becomes weak below these hyperbolic reflections which are interpreted to be associated with fractures or disruptions within the bedrock. The

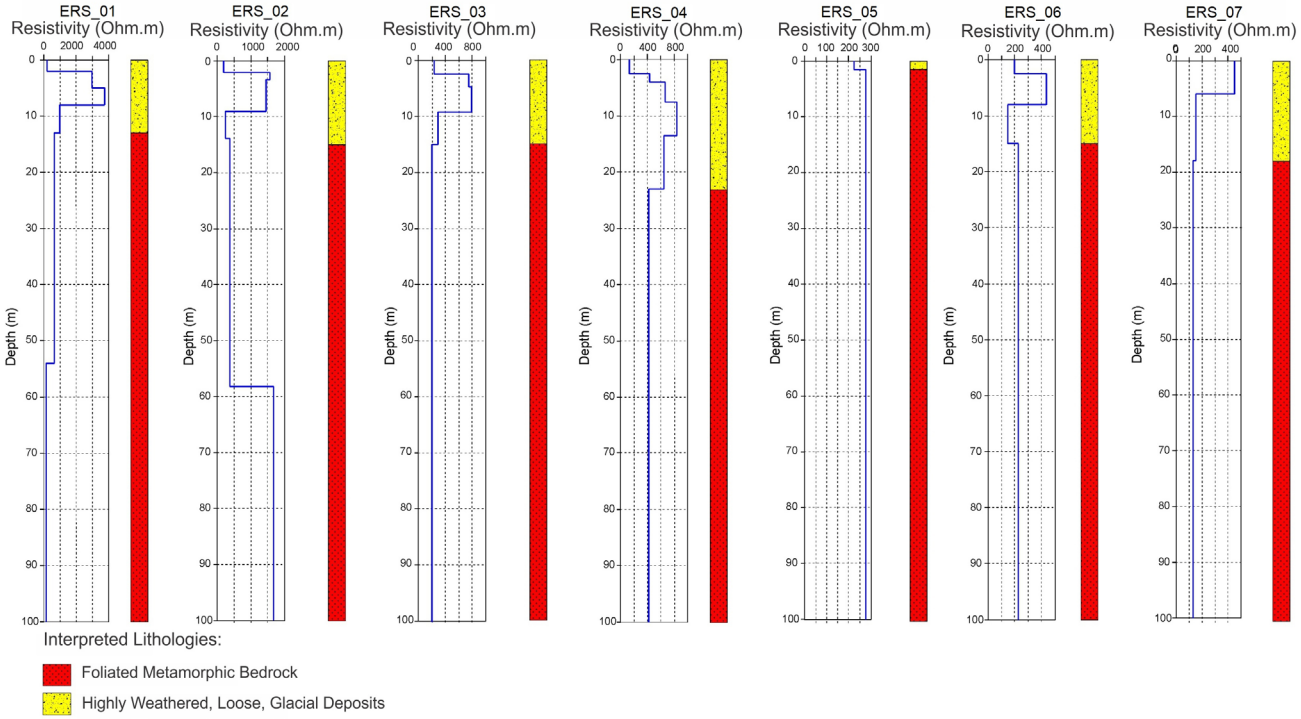

Figure 13: ERS data interpretation (ERS PROFILES 01-07)

same features are observed in the GPR_02 section (see **Figure 7**) between horizontal distances 06-20 m, 21-26 m, 35-40 m, 45-50 m, 75-80 m, 105-120 m, 120-160 m, 170-200 m and 3-6m BGL. An offset in the reflection is observed for the same section between the horizontal distances 165-170 m and 195-205 m, which lies directly above the interpreted hyperbolic reflections. The GPR_03 section (see **Figure 8**) has the hyperbolic reflections primarily seen between horizontal distances 7-18 m, 30-48 m, 57-65 m, 66-83 m, 108-121 m, 142-158 m, 171-188 m and 2-4m BGL. An offset in the reflection is seen for the same section between the horizontal distances of 52-58 m. The GPR_04 section (see **Figure 9**) has poor data quality between horizontal distances 0-40 m, 130-140 m due to a small depression and bad signal quality. The hyperbolic reflections are primarily seen between horizontal distances 70-110 m which is 3-6 m BGL. The GPR_05 section (see **Figure 10**) has the hyperbolic reflections primarily seen between horizontal distance 12-26 m, 28-40 m, 46-60 m, and 5-8 m BGL. The GPR_06 section (see **Figure 11**) has hyperbolic reflections primarily seen between horizontal distances 2-20 m, 32-45 m, 72-90 m, 100-110 m, 115-122 m, and 3-6 m BGL.

4.2 Electrical Resistivity Soundings (ERS)

The current and potential electrode spacing used in the field with the acquired apparent resistivity values are shown in **Table 1** as an example. The raw and processed ERS_01 to ERS_07 profiles are shown in **Figure 12**. The small white circles represent field apparent resistivity corresponding to the electrode spacing, black curve as apparent resistivity curve, red curve as the best fit model, and blue curve as the modeled subsurface layers. The subsurface is represented by 4 to 6 layers of material, each with a specific resistivity ranging from 20-3760 ohmmeter (Ω.m).

Table 1: ERS electrode configuration and apparent resistivity values used for ERS PROFILE 01

AB/2 (m)	MN/2 (m)	Apparent Resistivity (R) (Ω.m)
5	1	380.99
10	1	741.78
15	1	932.42
20	1	928.21
30	2	981.68
40	2	970.20
50	4	974.49
70	4	895.68
90	4	695.23

The ERS profiles are interpreted using the geological information from the study area and lithologic columns are prepared as shown in **Figure 13** below. The highly weathered and loose glacial deposits are characterized by high resistivities, whereas bedrock is relatively conductive.

5. Discussion

The top layer (Layer-1) is interpreted as a loose/fragmented material (such as silty, clayey sand with chunks

of detached and transported boulder size rock fragments) lying above the bedrock. This layer is characterized by parallel to sub-parallel reflection patterns down to an average approximate depth of 1.5–5m below ground level on all GPR sections. The complex reflection patterns in the top layer indicate highly heterogeneous material deposited in layers. The bottom layer (Layer-2) is interpreted as a bedrock formation, exposed on the surface at various parts of the landslide as foliated slates, phyllites, and schist of Yasin metasedimentary rock sequence. The GPR section's prominent feature is the bright and broad reflector at a depth of approximately 2–3 m between the two layers. The reflection strength decays sharply below this surface, suggesting a debonding between the layers. This debonding surface is interpreted as contact between the layers, where the two layers have loose contact facilitating the top layer to slip along the slope under unfavourable conditions such as rain or snowmelt. The hyperbolic reflections suggest the presence of faults or large fractures within the bedrock. The extension of these faults with depth is uncertain due to the GPR signal's decay. However, it is inferred from GPR data that the bedrock is highly deformed (fractured and faulted). The top layer also shows disruptions in reflection patterns, highlighted on all GPR sections. This disruption or offset in the reflection lies directly above the interpreted hyperbolic reflections (faults). It is interpreted that these fractured zones or faults have displacements, which lead to the disruption of strata in the top layer. Such zones are vulnerable to strong ground motions and when coupled with the debonded surface may trigger landslides, especially along higher slopes. The GPR_01 and GPR_02 sections (see **Figure 6** and **Figure 7**) representing the landslide's central part depicts the approximate depth of the bedrock as 2.5-3.0m. This site has a comparatively gentle slope with the lateral spreading of unconsolidated material at the top. Then the slope abruptly changes to approximately 75°-80° exposing the sheared foliated rocks at the slope face. The buried water pipeline (see **Figure 4**) has effectively controlled rock fragments, boulders, etc., in this part of the landslide. The GPR_03 section (see **Figure 8**) representing the western part of the landslide depicts the approximate average depth of bedrock as 1.0-1.5 m, which shows the overlying unconsolidated material has a lower thickness in this part of the landslide. However, the water channel is open and is confined to the metamorphosed rocks in this part of the landslide. The GPR_05 and GPR_06 sections (see **Figure 10** and **Figure 11**) representing the eastern part of the landslide depicts the approximate average depth of bedrock as 3.0-5.0m, which shows the unconsolidated material at the top has a higher thickness in this part of the landslide comparative to central and western sides. This part comprises glacial moraines, scree, weathered rock fragments, and clayey, silty soil. The site has an open water channel and has multiple cracks in the top unconsolidated surface layer with substantial openings up to 5m. The cracks are extended into the rock mass as shown by GPR data, but the depth of these cracks is uncertain due to the method's limitation. According to Rock Mass Rating (RMR), the foliated/sheared, low to medium-grade metamorphic slates or phyllites belongs to the Class V (very poor rock) (**Singh and Tamrakar., 2013**). The rocks at the site bounded between MKT and the Chalt Fault have already lost their shear strength due to intense tectonic activity (see **Figure 2**). Therefore, such highly deformed, sheared, and foliated rock is considered as soil (see **Figure 4**). The Mayoon landslide is considered to have a circular failure and is a rotational landslide (**Khan et al., 2019**).

The resistivity data is interpreted and developed into a lithological column (see **Figure 13**). The data is interpreted into a two-layered generalized model, i.e. a top layer (Layer-1) and a bottom layer (Layer-2). The top layer (Layer-1), is characterized by resistivity values ranging between 130 to 3760 Ω.m. This layer is interpreted as loose-fragmented material (such as silty, clayey sand with chunks of detached and transported boulder size rock fragments) lying above the bedrock. The high resistivity values (such as > 1000 Ω.m) suggest loose, disturbed, heterogeneous strata possibly deposited under the glacial settings. The bottom layer (Layer-2) is characterized by resistivity ranging between 20 and 660 Ω.m, and is interpreted as a bedrock. The lower resistivity values (such as < 100 Ω.m) suggest highly weathered rock formation, increasing the conductivity. In contrast, the higher resistivity values (such as > 100 Ω.m) suggest the presence of a competent bedrock. The ERS_04, 06, and 07 profiles have an interpreted depth of foliated metamorphic bedrock as 23 m, 16 m, and 18 m, respectively which shows the highly weathered, loose glacial deposits have more thickness in the eastern part of the landslide. The ERS_05 profile acquired at the toe of the central part of the landslide in the high school lawn has bedrock at an interpreted depth of 2 m. The ERS_01, 02, and 03 profiles have an interpreted depth of foliated metamorphic bedrock as 12 m, 15 m, and 15.5 m, respectively which shows the highly weathered, loose glacial deposits have more thickness at the toe of the landslide.

GPR data has suggested a debonding surface between the loose/fragmented top layer and the faulted/fractured bottom layer. The high resistivity value (130-3760 Ω.m) suggests the top layer has a loose and heterogeneous material whereas the low resistivity value (> 100 Ω.m) suggests the presence of bedrock. Such loose/fragmented rock material placed at higher slopes, with highly deformed, faulted/fractured bedrock in the presence of a possible slip surface may lead to a bigger landslide, particularly during heavy rains, snowmelt, and high seismic activity.

6. Conclusions

An attempt has been made to evaluate the Mayoon landslide's subsurface using geophysical techniques, in-

cluding GPR and ERS. The landslide is divided into three parts, i.e. the eastern part, the central part, and the western part (see **Figure 5**). The main conclusions are summarized as follows:

1. the GPR data is interpreted as a two-layered subsurface model. The top layer (Layer-1) is characterized by parallel to sub-parallel reflections and is associated with loose material comprised of silty clayey sand and fragmented rocks deposited in a glacial environment. The bottom layer (Layer-2) is a foliated and highly deformed bedrock;
2. contact between Layer-1 and Layer-2 is highlighted as a bright reflection, suggesting the contact is debonded between the two layers. Hyperbolic reflections are seen within the bedrock, which suggests the presence of fractures. The extension of fractures with depth is uncertain as GPR data lose resolution and the signal decays with depth. The top layer also shows a disruption in reflectors directly above the fractures/faults, suggesting a possible movement during intense seismic activity in the future;
3. the landslide's central part has an approximate average depth of bedrock as 2.5-3.0 m and has a concealed buried water pipeline. The lower thickness of the top layer with the concealed water pipeline marks this part of the landslide in medium-high vulnerability. The western part of the landslide has an approximate average depth of bedrock as 1.0-1.5 m. The open water channel is confined to the metamorphosed rocks in this part of the landslide. The overall approximate slope of 55-60 degrees with the bedrock's exposure at the surface marks this part of the landslide in low-medium vulnerability. The eastern part of the landslide has an approximate average depth to bedrock of 3.0-5.0 m, which shows the top layer has a higher thickness compared to the landslide's central and western parts. The open water channel has a continuous water seepage in the clayey, silty topsoil layer, which marks this part of the landslide as highly vulnerable;
4. the ERS data shows highly variable resistivity within the top layer, suggesting a heterogeneous setup. The high resistivity is associated with loose, fragmented material deposited under glacial settings. The loose, fragmented material lying above the faulted/fractured bedrock coupled with debonded surface pose a significant hazard to generate a landslide under unfavourable conditions, such as high-intensity rainfall and/or seismic activity;
5. the landslide is considered highly vulnerable due to the highly fractured/sheared bedrock, the open water channel, extreme freeze and thaw cycles, and high seismicity in the region.

Acknowledgments

This research is part of a Ph.D. research work. Qasim ur Rehman would like to thank the National Centre of Excellence in Geology, University of Peshawar, Pakistan, for providing a laboratory space and field logistics.

7. References

Agliardi, F., Crosta, G.B., Frattini, P. and Malusà, M.G. (2013): Giant non-catastrophic landslides and the long-term exhumation of the European Alps. Earth and Planetary Science Letters, 365, 263–274.

Ahmed, K.A., Khan, S., Sultan, M., Nisar, U. Bin, Mughal, M.R. and Qureshi, S.N. (2020): Landslides assessment using geophysical and passive radon exhalation detection techniques in Murree Hills, northern Pakistan: Implication for environmental hazard assessment. Journal of *Earth System Science,* 129, 53-71.

Ali, S., Biermanns, P., Haider, R. and Reicherter, K. (2019): Landslide susceptibility mapping by using a geographic information system (GIS) along the China–Pakistan Economic Corridor (Karakoram Highway), Pakistan. Natural Hazards and Earth System Sciences,19, 999-1022.

Alsharahi, G., Mint, M.M.A., Faize, A., Driouach, A., (2016). Modeling and simulation resolution of ground-penetrating radar antennas. Journal of Electromagnetic Engineering and Science, 16, 182–190.

Bacha, A.S., Shafique, M. and Vander, WH. (2018): Landslide inventory and susceptibility modeling using geospatial tools, in Hunza-Nagar valley, northern Pakistan. Journal of *Mountain Science*,15, 1354–1370.

Bignold, S.M., and Treloar, P.J. (2003): Northward subduction of the Indian Plate beneath the Kohistan island arc, Pakistan Himalaya: new evidence from isotopic data. Journal of Geological Society, London,160, 377–384.

Borecka, A., Herzig, J. and Durjasz-Rybacka, M. (2015): Ground penetrating radar investigations of landslides: a case study in a landslide in Radziszów. Studia Geotechnica et Mechanica, 37, 11–18.

Brezhnev, R.V., Maglinets, Y.A. and Raevich, K.V. 2020: An Interactive Environment for Modeling the Processes of ERS Data Processing and Analysis. CEUR Workshop Proceedings, 61–67.

Cardarelli, E. and De Donno, G. (2017): Multidimensional electrical resistivity survey for bedrock detection at the Rieti Plain (Central Italy). Journal of Applied Geophysics, 141, 77–87.

Dewey, J., Cande, S. and Pitman, W. (1989): The tectonic evolution of the India/Eurasia collision zone. Eclogae Geologicae Helvetiae, 82, 717–734.

DiPietro, J.A. and Pogue, K.R. (2004): Tectonostratigraphic subdivisions of the Himalaya: A view from the west. Tectonics, 23, 1-20.

Dortch, J.M., Owen, L.A., Haneberg, W.C., Caffee, M.W., Dietsch, C. and Kamp, U. (2009): Nature and timing of large landslides in the Himalaya and Transhimalaya of northern India. *Quaternary Science* Reviews, 28, 1037–1054.

Gallo, F. and Lavé, J. (2014): Evolution of a large landslide in the High Himalaya of central Nepal during the last half-century. Geomorphology, 223, 20–32.

Hewitt, K. (1998): Catastrophic landslides and their effects on the Upper Indus streams, Karakoram Himalaya, northern Pakistan. Geomorphology, 26, 47–80.

Hungr, O., Leroueil, S., Picarelli, L., (2014). The Varnes classification of landslide types, an update. Landslides 11(2), 167–194.

Hussain, F. and Hussain, M. (2017): China-Pak economic corridor (CPEC) and its geopolitical paradigms. *International Journal* of *Social Sciences*, 1, 79–95.

Irshad, M.S. (2015): One belt and one road: dose China-Pakistan economic corridor benefit for Pakistan's economy?. Journal of Economics and Sustainable Development, 6, 200-207.

Jagoutz, O. and Schmidt, M.W. (2012): The formation and bulk composition of modern juvenile continental crust: The Kohistan arc. Chemical Geology, 298, 79–96.

Jones, D.K.C. (1992): Landslide hazard assessment in the context of development, Geohazards, 10, 117–141.

Jongmans, D. and Garambois, S. (2007): Geophysical investigation of landslides: Bulletin de la Société géologique de France, 178, 101–112.

Kannaujiya, S., Chattoraj, S.L., Jayalath, D., Bajaj, K., Podali, S. and Bisht, M.P.S. (2019): Integration of satellite remote sensing and geophysical techniques (electrical resistivity tomography and ground penetrating radar) for landslide characterization at Kunjethi (Kalimath), Garhwal Himalaya, India. Natural Hazards, 97, 1191–1208.

Khan, G., Karim, P., Ahmad, Z., Qureshi, J.A., Ali, M., ur Rehman, S., Alam, M., Khan, A.A. and Begum, F. (2019): Landslide Hazard Risk Assessment and Landuse Planning of Mayoon, Hunza, GilgitBaltistan, Pakistan. International Journal of Economic and Environmental. Geology, 10, 30–34.

Ling, C., Xu, Q., Zhang, Q., Ran, J., Lv, H., (2016). Application of electrical resistivity tomography for investigating the internal structure of a translational landslide and characterizing its groundwater circulation (Kualiangzi landslide, Southwest China). Journal of Applied Geophyics. 131, 154–162.

Lissak, C., Maquaire, O., Malet, J.-P., Lavigne, F., Virmoux, C., Gomez, C. and Davidson, R. (2015): Ground-penetrating radar observations for estimating the vertical displacement of rotational landslides. Natural Hazards Earth System Science, 15, 1399–1406.

Makhdoom, A.S., Shah, A.B. and Sami, K. (2018): Pakistan On The Roadway To Socio-Economic Development: A Comprehensive Study Of China Pakistan Economic Corridor (Cpec). The Government Research Journal of Political Science, 6, 37-46.

Meric, O., Garambois, S., Jongmans, D., Wathelet, M., Chatelain, J.-L. and Vengeon, J.M. (2005): Application of geophysical methods for the investigation of the large gravitational mass movement of Séchilienne, France. Canadian *Geotechnical* Journal, 42, 1105–1115.

Mondal, S.K., Sastry, R.G., Pachauri, A.K. and Gautam, P.K. (2008): High resolution 2D electrical resistivity tomography to characterize active Naitwar Bazar landslide, Garhwal Himalaya, India Current Science, 871–875.

Perrone, A., Lapenna, V. and Piscitelli, S. (2014): Electrical resistivity tomography technique for landslide investigation: a review. Earth-Science Reviews 135, 65–82.

Petterson, M.G. (2010): A review of the geology and tectonics of the Kohistan island arc, north Pakistan. Geologocal Society London, Specical Publications, 338, 287–327.

Regmi, A.D., Yoshida, K., Cui, P. and Hatano, N. (2017): Development of Taprang landslide, West Nepal. Landslides, 14, 929–946.

Rehman, M.U., Zhang, Y., Meng, X., Su, X., Catani, F., Rehman, G., Yue, D., Khalid, Z., Ahmad, S. and Ahmad, I. (2020): Analysis of landslide movements using interferometric synthetic aperture radar: A case study in Hunza-Nagar Valley, Pakistan. Remote Sensing, 12,12, 2054.

Searle, M.P., Khan, M.A., Fraser, J.E., Gough, S.J. and Jan, M.Q. (1999): The tectonic evolution of the Kohistan-Karakoram collision belt along the Karakoram Highway transect, north Pakistan. Tectonics, 18, 929–949.

Searle, M.P., Windley, B.F., Coward, M.P., Cooper, D.J.W., Rex, A.J., Rex, D., Tingdong, L., Xuchang, X., Jan, M.Q. and Thakur, V.C. (1987): The closing of Tethys and the tectonics of the Himalaya. *Geological Society of America Bulletin*, 98, 678–701.

Shah, S.H.A., Arif, M., Asif, M.E., Safdar, M. (2019): Influence of Granite Cutting Waste Addition on the Geotechnical Parameters of Cohesive Soil. International Journal of Engineering Research and Advance Technology, 5, 64–74.

Shah, S.H.A., Arif, M., Sabir, M.A., Iqbal, J., (2020a): in-situ stabilization of clays with lime, dolerite and quartzite powders. Acta Geodynamica et Geomaterialia, 17, 341–353.

Shah, S.H.A., Arif, M., Sabir, M.A., ur Rehman, Q., (2020b): Impact of Igneous Rock Admixtures on Geotechnical Properties of Lime Stabilized Clay. Civil and Environmental Engineering, 16, 329–339.

Shang, Y., Yang, Z., Li, L., Liao, Q. and Wang, Y. (2003): A super-large landslide in Tibet in 2000: background, occurrence, disaster, and origin. Geomorphology, 54, 225–243.

Singh, J. L., & Tamrakar, N. K. (2013). Rock mass rating and geological strength index of rock masses of Thopal-Malekhu river areas, central Nepal lesser himalaya. Bulletin of the Department of Geology, 16, 29–42.

Telford, William Murray, Telford, W M, Geldart, L.P., Sheriff, R.E. and Sheriff, R.E. (1990): Applied geophysics. Cambridge university press, 107 p.

Xie, M., Zhao, W., Ju, N., He, C., Huang, H. and Cui, Q. (2020): Landslide evolution assessment based on InSAR and real-time monitoring of a large reactivated landslide, Wenchuan, China. Engineering Geology, 277, 105-131.

Yalcinkaya, E., Alp, H., Ozel, O., Gorgun, E., Martino, S., Lenti, L., Bourdeau, C., Bigarre, P. and Coccia, S. (2016): Near-surface geophysical methods for investigating the Buyukcekmece landslide in Istanbul, Turkey. Journal of Applied Geophysics,134, 23–35.

Zanchi, A. and Gaetani, M. (2011): The geology of the Karakoram range, Pakistan: the new 1: 100,000 geological map of Central-Western Karakoram. Italy Journal of Geoscience. 130, 161–262.

SAŽETAK

Geofizička istraživanja potencijalnoga klizišta u području Mayoon, distrikt Hunza, Gilgit-Baltistan, Pakistan

Klizište Mayoon u distriktu Hunza pripada skupini sporo razvijajućih, nekatastrofičnih klizišta. Važnost mu je porasla u nekoliko zadnjih godina nakon što se klizanje znatno ubrzalo. Cijelo područje obilježeno je visokim potresnim rizikom (zona 3, s najvećim ubrzanjem tla 2,4 – 3,2 m/s^2), a u skladu s pakistanskim propisima o gradnji. Snažni potresi u prošlosti pomaknuli su blokove metamorfnih stijena prema jugu i uzrokovali otvaranje brojnih pukotina u stijenama podine. Čelo i tijelo klizišta prekriveno je nekonsolidiranim materijalom te ima pukotine različitih širina i dužina. Prostor klizišta istražen je neinvazivnim geofizičkim tehnikama poput georadara i mjerenja električne otpornosti. Podzemlje je prikazano dvoslojnim modelom. Prvi sloj (1) predstavljen je snažnim reflektorom i vrlo promjenjivom otpornošću. Sastavljen je od rastresitih, vrlo heterogenih, fragmentiranih materijala taloženih tijekom glacijala preko stijenske podine. Ispod je drugi sloj (2) obilježen hiperboličkim refleksima te umjerenom otpornošću i pruža se unutar folijacijskih, metamorfnih stijena. Oblik refleksa upozorava na rasjede i pukotine podine, no oni se teško prate s povećanjem dubine. Otpornost također upućuje na trošenje i folijaciju. Refleksi u sloju 1 prekidaju se iznad rasjeda i pukotina upozoravajući na moguće gibanje. Snažni refleksi između dvaju slojeva naglašavaju postojanje granice između njih. Rastresiti materijal u sloju 1, zajedno s postojanjem takve granice, predstavlja znatan rizik nastanka klizišta, posebice u rizičnim uvjetima poput olujnoga pljuska ili potresa.

Ključne riječi:
georadar, električna otpornost, hiperbolični refleksi, razdvojene površine, borana podina

Author's contribution

This study was designed, performed, and compiled by **Qasim ur Rehman** as the principal investigator and is a part of his Ph.D. research. The conceptual and technical guidance for all aspects of the research was given by Supervisor, **Dr. Waqas Ahmed**, and Co-Supervisor, **Dr. Muhammad Waseem**. **Dr. Sarfraz Khan** and **Mr. Syed Husnain Ali Shah** assisted in GPR and ERS data acquisition. **Mr. Syed Husnain Ali Shah** also participated in the sequence alignment of the manuscript. **Dr. Asam Farid** assisted in analyzing the GPR and ERS data. All authors read and approved the final manuscript.